Reshaping Particle Configurations by Collisions with Rigid Objects

Shiva Shahrokhi, Haoran Zhao, and Aaron T. Becker

Abstract— **Consider many particles actuated by a global external field (e.g. gravitational or magnetic fields). This paper presents analytical results using workspace obstacles and global inputs to reshape such a group of particles. Shape control of many particles is necessary for conveying information, construction, and for navigation. In the absence of workspace obstacles, it is not possible to change the relative position of particles. First we show how the particles' characteristic angle of repose can be used to reshape the particles by controlling angle of attack and the magnitude of the driving force. These can then be used to control the force and torque applied to a rectangular rigid body. Next, we examine the full set of stable achievable first and second moments for the shape of a particle group in two canonical environments: a square and a circular workspace. Then we show how workspaces with linear boundary layers can be used to achieve a more rich set of mean and variance configurations. We conclude with hardware experiments investigating shape control using angle of repose and hardware boundaries.**

I. Introduction

This paper investigates the set of configurations that can be stably achieved for a large group of particles, all controlled by the same global force, in a workspace with rigid obstacles. Shape control of many particles is essential for navigation, construction, and conveying information. The small size of the particles makes it hard or even impossible to control each particle's position individually. Instead, these particles are often controlled with a single global control input. This work analyses interactions between the rigid obstacles and the particles to control the configuration of the particles.

The paper is arranged as follows. After a review of recent related work in Sec. II, Sec. III introduces angle of repose, a parameter of the particle swarm that can be used for shape control. Section IV provides analytical position control results of stable configurations in two canonical workspaces with frictionless walls. These results are limited in the set of shapes that can be generated. To extend the range of possible shapes, the section explores using linear boundary friction. Hardware experiments and results are presented in Sec. V. We end with directions for future research in Sec. VI.

II. Related Work

Controlling the relative position of many particles is necessary for a range of applications. Therefore, it has been a topic of research from a control perspective in both centralized and distributed approaches. This paper focuses

*This work was supported by the National Science Foundation under Grant No. [IIS-1553063] and [IIS-1619278].

Authors are with the Department of Electrical and Computer Engineering, University of Houston, Houston, TX 77204 USA {`sshahrokhi2, hzhao9@uh.edu, atbecker`}`@uh.edu`

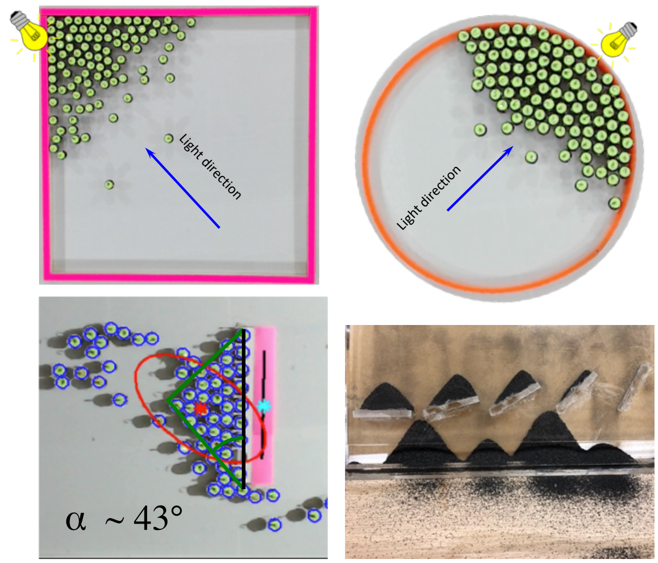

Fig. 1. Reshaping particles by collisions with rigid bodies. Top pictures illustrates using closed boundaries to reshape the particles. Bottom pictures illustrates angle of repose of different particles.

on centralized approach that apply the uniform control input to all the particles. To change the relative position of the particles, we need to break the symmetry caused by the uniform input. Symmetry can be broken using particles that respond differently to the uniform control signal, either through agent-agent reactions [3], or engineered inhomogeneity [4]–[6]. The magnetic gradients of MRI scanners are *uniform*, meaning the same force is applied everywhere in the workspace [7]. This work assumes a uniform control with homogenous particles, as in [8], and breaks the control symmetry using obstacles in the workspace. While in [2] we showed how to control the mean position and variance through repeated collisions with the workspace, this paper focuses on stable configurations. In [**?**] we showed that single obstacle can be used to rearrange n particles using an $O(n^2)$-time algorithm. In other previous work, we gave algorithms that could adjust the position of n particles in an environment with walls that have non-slip contacts [1] in $O(n^2)$-time. We assumed that if a particle is pushed into a wall, it will not move until a uniform input pulls it from the wall.

Alternative techniques rely on non-uniform inputs, such as artificial force-fields. Much recent work in magnet control has focused on exploiting inhomogeneities in the magnetic field to control multiple micro particles using gradient-based

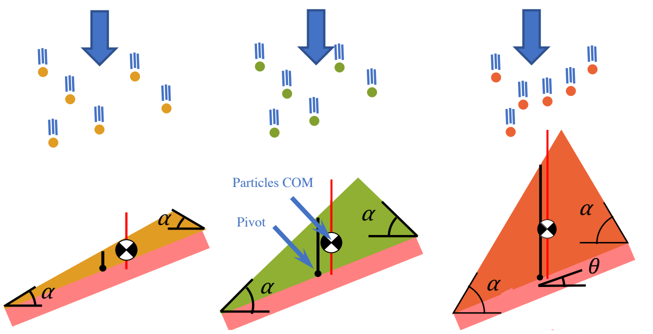

Fig. 2. If particles move faster than the (pink) rod, some particles slide past the rod, but the ones that remain pile up in a shape characterized by the angle of repose α, which is particular to the particle type.

pulling [9], [10]. Using large-scale external magnetic fields makes it challenging to independently control more than one microrobot unless the distance between the electromagnetic coils is at the same length scales as the robot workspace [9]–[11].

III. Angle of Repose

Consider a swarm of granular particles applying force to a rod. If the rod moves slower than the particles, some particles will slide past the rod, but other particles will build up behind the rod in a characteristic triangular shape defined by a steepest angle of descent perpendicular to the direction of particle motion. This piling up is common to all granular media, and the angle formed perpendicular to the angle of attack is the *angle of repose*. Three different values of angle of repose is shown in Fig. 2. The center of mass of the rod is in the middle of the rod, but center of mass of the granular particles changes for different values of angle of repose. By measuring the angle of repose for the particles shown in the top plot of Fig. 3, we can estimate the force and torque that the swarm is applying to the rod as a function of the rod's length, the angle of repose, and orientation of the rod. In this plot, particulate is moving in the $-y$ direction, and the rods are tilted at $\theta = \{-45, -22.5, 0, 22.5, 45\}^{\circ}$ with respect to the x axis. A thin black line extends upwards from the rod COM, and the COM of the particulate is shown by a white and black disk. More particulate is heaped on the right side of the rod for positive θ and more on the left side for negative θ. This uneven particulate generates a restoring torque. We define the angle of repose as α, the rod's orientation relative to 90° from the particle movement vector as θ, and the rod's length as ℓ.

A. Force and Torque

By integrating over the triangular shape, the force applied to the rod (when a unit area of particles produces 1 N of force) is ?? TODO: Aaron INsert the integral

$$F(\theta,\alpha,\ell) = \begin{cases} \frac{\ell^2\left(\cos(2\theta)-\cos(2\alpha)\right)}{8\cos(\alpha)\sin(\theta)} & -\alpha < \theta < \alpha \\ 0 & \text{otherwise}\ . \end{cases} \qquad (1)$$

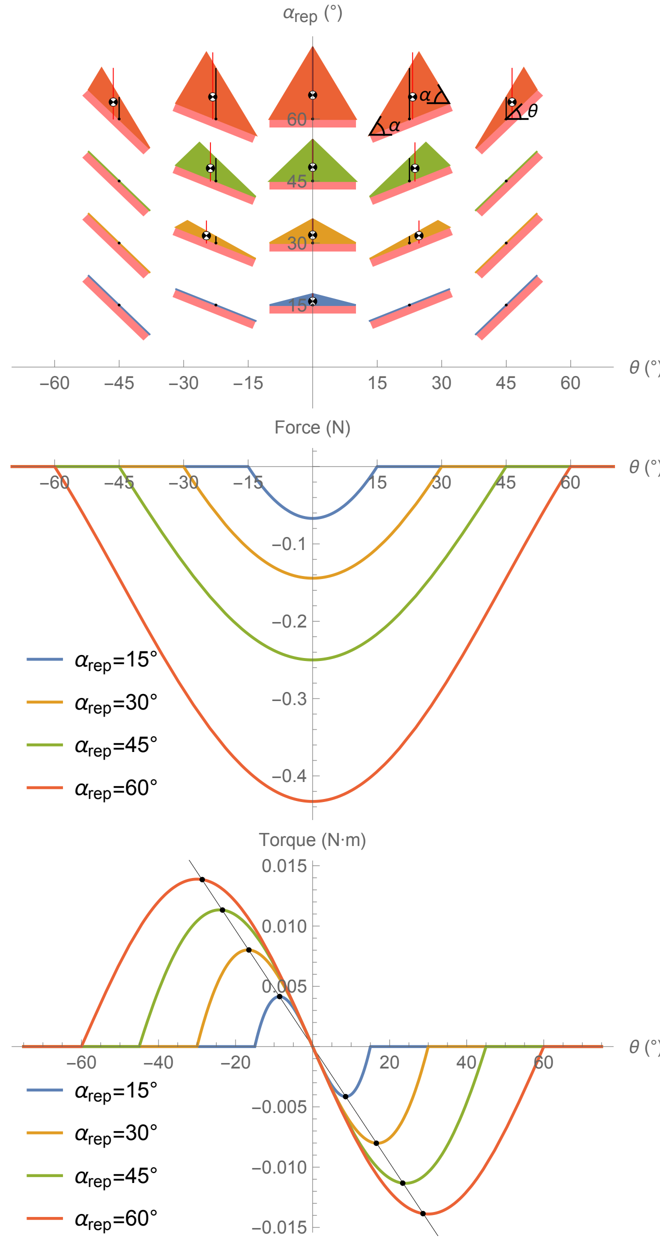

Fig. 3. Top plot shows colored particulate heaped up on pink-colored long rods. Middle plot shows the force applied to the rod and bottom the torque as a function of θ for four angle of repose values. The maximum torque values from (3) are shown with black dots, producing a line that is approximately $-\ell^3/36\theta_{t_{\max}}$.

The force for different angle of repose values are shown in the middle plot of Fig. 3, with the rod length $\ell = 1$. Torque will also be similarly defined as

$$\tau(\theta,\alpha,\ell) = \begin{cases} \frac{\ell^3\left(\cos(2\alpha)-\cos(2\theta)\right)\sin(\theta)}{48\sin^2(\alpha)} & -\alpha < \theta < \alpha \\ 0 & \text{otherwise}\ . \end{cases} \qquad (2)$$

Torque is shown in the bottom plot of Fig. 3 with the rod length $\ell = 1$. Given sufficient particles to pile up to the angle of repose, this torque tends to stabilize the object to be perpendicular to the pushing direction. Force is maximized with $\theta = 0$, but the θ value that maximizes torque is a function of α and is defined as

$$\theta_{t_{\max}} = \frac{\sin(\alpha)}{\sqrt{3}}. \tag{3}$$

To maximize the torque a particulate swarm applies on a thin rod, the swarm should move in the direction $-\theta_{t_{\max}} - 90°$ with respect to the long axis of the rod.

B. Shape Control

Often the angle of the rigid rod is given, but we can choose the desired approach direction β. This section examines the possible shapes that can be generated given a rigid rod of length ℓ, an angle of repose α, and an approach angle where the swarm moves at angle relative to the long axis of the rod β.

Computing means, variances, covariance, and correlation requires integrating over R, the region containing the swarm and are calculated as

$$A = \iint_R dx\,dy,\ \bar{x} = \frac{\iint_R x\,dx\,dy}{A},\ \bar{y} = \frac{\iint_R y\,dx\,dy}{A}, \tag{4}$$

$$\sigma_x^2 = \frac{\iint_R (x-\bar{x})^2\ dx\,dy}{A},\ \sigma_y^2 = \frac{\iint_R (y-\bar{y})^2\ dx\,dy}{A}, \tag{5}$$

$$\sigma_{xy} = \frac{\iint_R (x-\bar{x})(y-\bar{y})\ dx\,dy}{A},\ \rho_{xy} = \frac{\sigma_{xy}}{\sqrt{\sigma_x^2\sigma_y^2}}. \tag{6}$$

Using these equations, we can calculate the representative shape statistics as a function of approach angle β, a one degree-of-freedom set. For instance, the area A of the particles is (1) with $\theta = \beta + \pi/2$, and the y-variance is

$$\sigma_y^2(\alpha,\beta,\ell) = \frac{1}{72}\left(\cot(2\alpha) + \frac{\cos(2\beta)}{\cos(2\alpha)}\right)^2. \tag{7}$$

Representative results are shown in Fig. 4.

IV. Shape Control using Rigid Boundaries

Shape control using angle of repose only considers the particles that pile up on the object, but most of the particles pass by. This section instead focuses on shape control of the entire group when all the particles are pushed against rigid boundaries, starting by examining analytically all possible configurations in two canonical configuration spaces, and then examining the effect of boundary layer friction.

A. Using boundaries: stable configurations of a swarm

One method to control a swarm's shape in a bounded workspace is to simply push in a given direction until the swarm conforms to the boundary. Like fluid settling in a tank, the stable final configuration minimizes potential energy by forming a configuration with a level surface perpendicular to the push direction. The set of final configurations are parametrized by a single degree of freedom, the global input angle β.

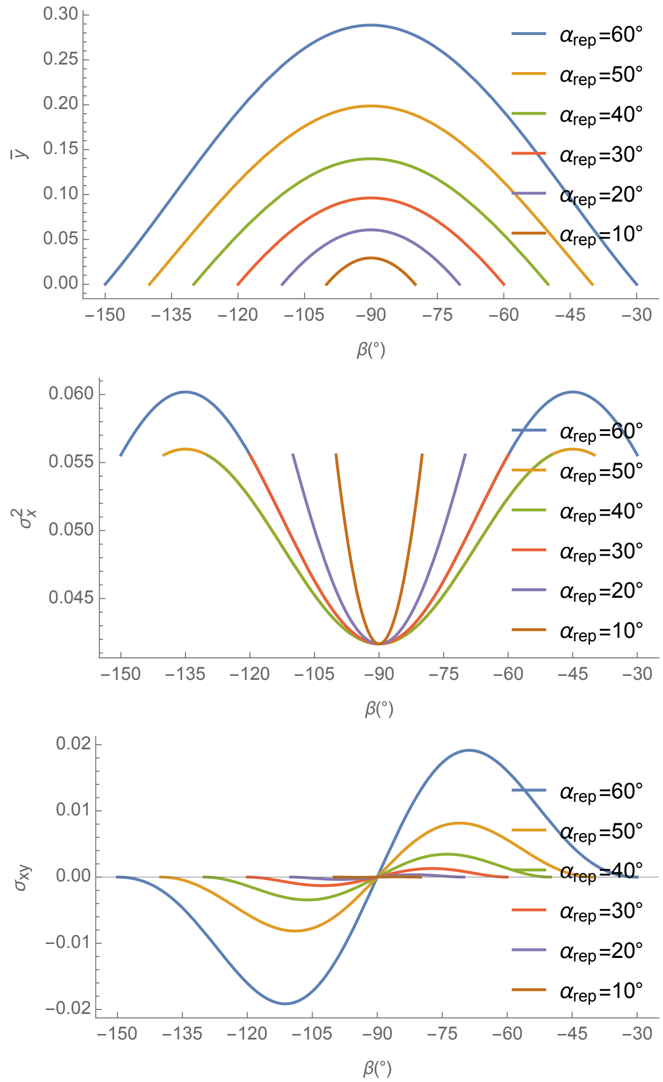

Fig. 4. Each plot shows a statistic of the swarm shape for several angle of repose α values as a function of the approach angle β with $\ell = 1$. Top plot shows the mean y coordinate $\bar{y}$, middle plot shows x-variance σ_x^2, and bottom plot shows the covariance σ_{xy}.

a) Square workspace: We first examine the mean $(\bar{x},\bar{y})$, covariance $(\sigma_x^2,\sigma_y^2,\sigma_{xy})$, and correlation ρ_{xy} of a large swarm of particles as they move inside a square workspace under the influence of a force pulling in the direction β. The swarm is large, but the particles are small in comparison, and together occupy a constant area A, $A \in [0,1]$. Under a global input, the swarm moves to a side of the workspace and forms a polygonal shape that minimizes potential energy, as shown in Fig. 5.

The range for the global input angle β is $[0,2\pi)$. In this range, the swarm assumes eight different polygonal shapes. These shapes alternate between triangles and trapezoids when the area $A<1/2$, and between squares with one corner removed and trapezoids when $A>1/2$.

The region of integration R is the polygon containing the swarm. For example, if $A < 1/2$ and the force angle is β, the mean when R is a triangular region in the lower-left corner

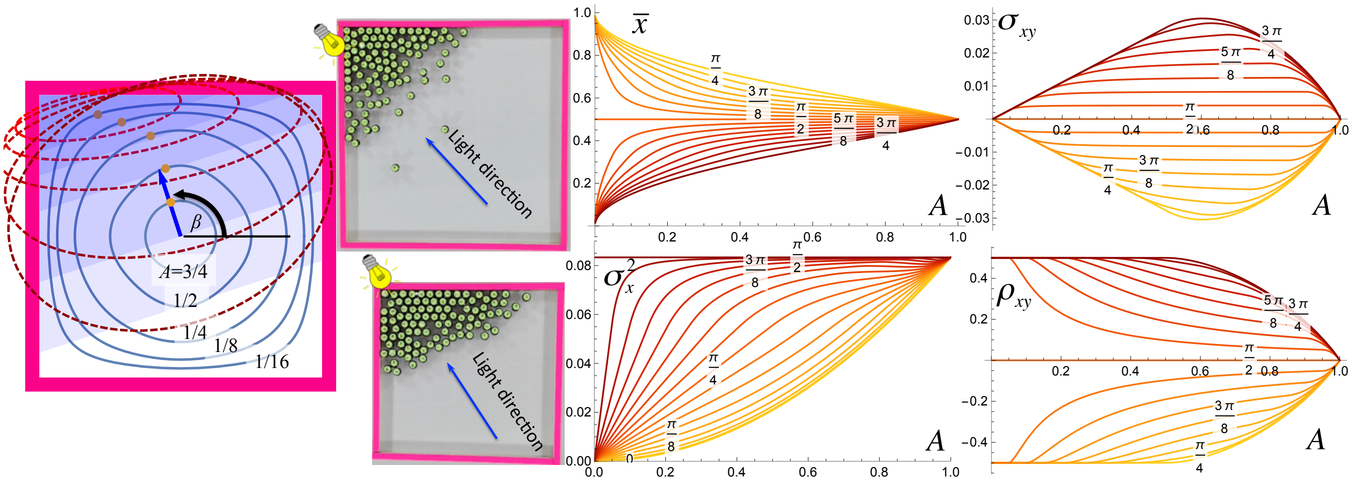

Fig. 5. Pushing the swarm against a square boundary wall allows limited control of the shape of the swarm, as a function of swarm area A and the commanded movement direction β. Left plot shows locus of possible mean positions for five values of A. Center shows two corresponding arrangements of kilobots. At right is $\bar{x}(A), \sigma_{xy}(A), \sigma_x^2(A)$, and $\rho_{xy}(A)$ for a range of β values. See online interactive demonstration at [12].

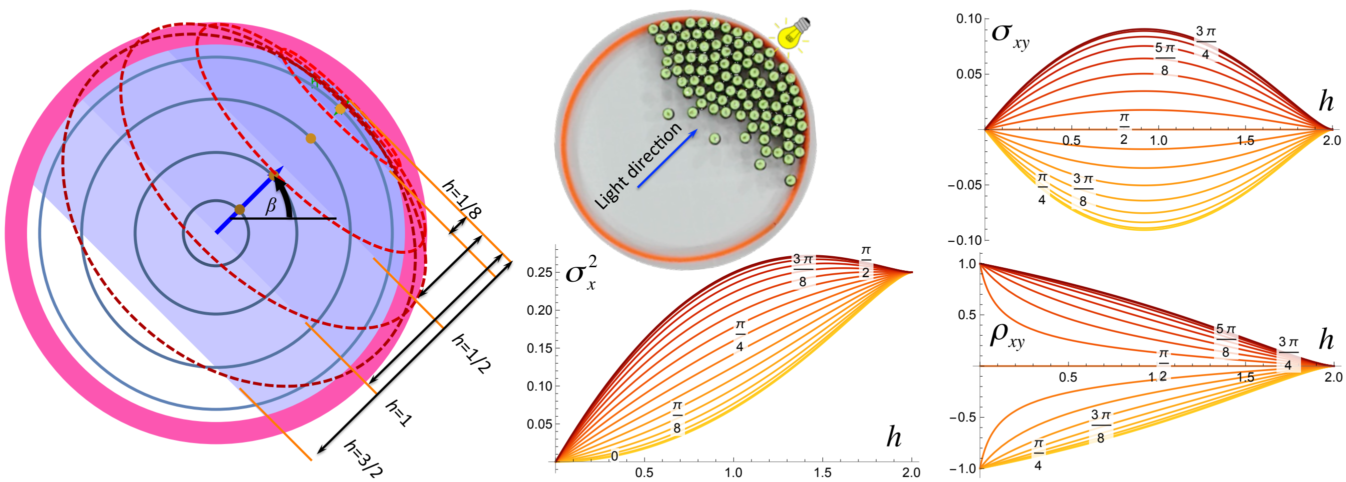

Fig. 6. Pushing the swarm against a circular boundary wall allows limited control of the shape of the swarm, as a function of the fill level h and the commanded movement direction β. Left plot shows locus of possible mean positions for four values of h. The locus of possible mean positions are concentric circles. At right is $\sigma_{xy}(h), \sigma_x^2(h)$, and $\rho_{xy}(h)$ for a range of β values. See online interactive demonstration at [13].

is:

$$\bar{x}(A,\beta) = \frac{\int_0^{\sqrt{2A\tan(\beta)}} \left(\int_0^{\cot(\beta)\left(\sqrt{2A\tan(\beta)}-x\right)} dy \right) x\, dx}{A} = \frac{\sqrt{2}}{3}\sqrt{A\tan(\beta)}, \tag{8}$$

$$\bar{y}(A,\beta) = \frac{\int_0^{\sqrt{2A\tan(\beta)}} \left(\int_0^{\cot(\beta)\left(\sqrt{2A\tan(\beta)}-x\right)} y\, dy \right) dx}{A} = \frac{\sqrt{2}}{3}\sqrt{A\cot(\beta)}. \tag{9}$$

The set of configurations are summarized in Fig. 5. For the full equations and demonstration code, see [12]. A few highlights are that the correlation is maximized $\pm 1/2$ when the swarm is in a triangular shape. The covariance of a triangle is always $\pm(A/18)$. Variance is minimized in the direction of β and maximized orthogonal to β when the swarm is in a rectangular shape. The range of mean positions are maximized when A is small.

b) Circular workspace: Though rectangular boundaries are common in artificial workspaces, biological workspaces are usually rounded. Similar calculations can be made for a circular workspace. The workspace is a circle centered at (0,0) with radius 1 and thus area π. For notational simplicity, the swarm is parameterized by the global control input signal β and the fill-level $h \in [0,2]$. Under a global input, the particle swarm fills the region under a chord with area

$$A(h) = \arccos(1-h) - (1-h)\sqrt{(2-h)h}. \tag{10}$$

For a circular workspace, the locus of mean positions are aligned with β and the mean position is at radius $r(h)$ from the center which is

$$r(h) = \frac{2(-(h-2)h)^{3/2}}{3\left(\sqrt{-(h-2)h}(h-1) + \arccos(1-h)\right)}. \tag{11}$$

Variance $\sigma_x^2(\beta,h)$ is maximized at $\beta=\pi/2+n\pi$ and $h\approx 1.43$, while covariance is maximized at $\beta=\pi 3/4+n\pi$ and $h\approx 0.92$. For small h values, correlation approaches ± 1. Results are displayed in Fig. 6. For the full equations and demonstration code, see [13].

B. Using boundaries: friction and boundary layers

Global inputs move a swarm uniformly. Shape control requires breaking this uniform symmetry. A swarm inside an axis-aligned rectangular workspace can reduce variance normal to a wall by simply pushing the swarm into the boundary. If the swarm can flow around each other, pushing the swarm into a boundary produces the limited set of configurations presented in Sec. IV-A. Instead of pushing our particles directly into a wall, the following sections examine an oblique approach using boundaries that generate friction with the particles. These frictional forces are sufficient to break the symmetry caused by uniform inputs. Particles touching a wall have a friction force that opposes movement along the boundary. This causes particles along the boundary to move more slowly than particles in free-space.

Let the control input be a vector force $\vec{F}$ with magnitude F and orientation θ with respect to a line perpendicular to and into the nearest boundary. N is the normal or perpendicular force between the particle and the boundary. The force of friction F_f is nonzero if the particle is in contact with the boundary and $\sin(\theta)<0$. The resulting net force on the particle, $F_{forward}$, is aligned with the wall and given by

$$\begin{aligned} F_{forward} &= F\sin(\theta)-F_f,\\ \text{where } F_f &= \begin{cases}\mu_f N, & \mu_f N < F\sin(\theta)\\ F\sin(\theta), & \text{else}\end{cases}\\ \text{and } N &= F\cos(\theta). \end{aligned} \tag{12}$$

Fig. 7 shows the resultant forces on two particles when one is touching a wall. Though each receives the same inputs, they experience different net forces. For ease of analysis, the following algorithms assume μ_f is infinite and particles touching the wall are prevented from sliding along the wall. This means that if one particle is touching the wall and another particle is free, the touching particle will not move when the control input is parallel or into the wall. There are many alternate models of friction that also break control symmetry. Fig. 7c shows fluid flow along a boundary. Fluid in the free-flow region moves uniformly, but flow decreases to zero in the boundary layer [14]. Force in such a system can be calculated as

$$F_{forward}(y) = F - F_f\begin{cases}\frac{h-y}{h}, & y<h\\ 0, & \text{else}\end{cases}. \tag{13}$$

C. Maximizing correlation using wall friction

Assume an obstacle-free, bounded, unit-size, square workspace. As shown in Fig. 5, the maximum correlation occurs when the swarm is pushed in the direction $\beta=3\pi/4$. This correlation as a function of swarm area A is never larger than 1/2, and the maximum correlation decays to 0 as A grows to 1. By (6), this maximum correlation is

$$\rho_{xy}=\begin{cases}\frac{1}{2}, & 0\le A\le\frac{1}{2}\\ \frac{3A(2(A-2)A+1)}{4A^3-24A+\sqrt{2}(12A-12)\sqrt{1-A}+17}-1, & \frac{1}{2}\le A\le 1\end{cases}. \tag{14}$$

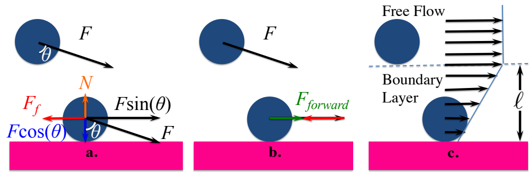

Fig. 7. (a,b) Wall friction reduces the force for going forward $F_{forward}$ on a particle near a wall, but not for a free particle. (c) velocity of a fluid reduces to zero at the boundary.

If friction obeys the linear boundary layer model of (13) with boundary layer thickness h and maximum friction F_f equal to the maximum applied force F, we can generate larger correlations. If the swarm size is smaller than $A\approx 0.43$ and the boundary layer is sufficiently thick we can generate correlations larger than 1/2 using boundary friction.

Assume that the swarm is initialized in the lower-left corner, in a rectangle of width w and height A/w. Such a rectangular configuration can be accomplished using the variance controllers from [15]. If the swarm is then commanded to move a distance L to the right, components of the swarm outside the boundary friction layer of height h move further than components near the boundary. The swarm is contained in a region R composed of no more than three stacked components: at bottom a parallelogram inclined to the right top, at middle a rectangle, and at top a parallelogram inclined to the left top. These regions can be defined by the rectangle's left side, bottom, and top:

$$\begin{aligned} r_{\text{left}} &= \min\left(L, 1-w\right),\\ r_{\text{bottom}} &= \min\left(\frac{A}{w}, h\frac{r_{\text{left}}}{L}\right) \text{ and}\\ r_{\text{top}} &= \min\left(\frac{A}{w}, 1-h\frac{r_{\text{left}}}{L}\right). \end{aligned} \tag{15}$$

If $\frac{A}{w}\le r_{\text{top}}$ the top parallelogram has no area. Similarly, if $r_{\text{top}}\le r_{\text{bottom}}$ the rectangle has no area. The mean, variance, and correlation are calculated using (4), (5), and (6) over the region R:

$$\begin{aligned} \iint_R f(x,y)\,dx\,dy = &\int_0^{r_{\text{bottom}}}\int_{\frac{L}{h}y}^{\frac{L}{h}y+w} f(x,y)dx\,dy \\ &+\int_{r_{\text{bottom}}}^{r_{\text{top}}}\int_{r_{\text{left}}}^{r_{\text{left}}+w} f(x,y)dx\,dy\\ &+\int_{r_{\text{top}}}^{\frac{A}{w}}\int_{-\frac{L(y-r_{\text{top}})}{h}+r_{\text{left}}}^{r_{\text{left}}+w-\frac{L(y-r_{\text{top}})}{h}} f(x,y)dx\,dy. \end{aligned} \tag{16}$$

Given an environment parameterized by A and h, efficient correlation control consists of choosing the w, L pair that generates the desired positive correlation. Negative correlations can be generated by initializing the swarm in the upper left, or lower right.

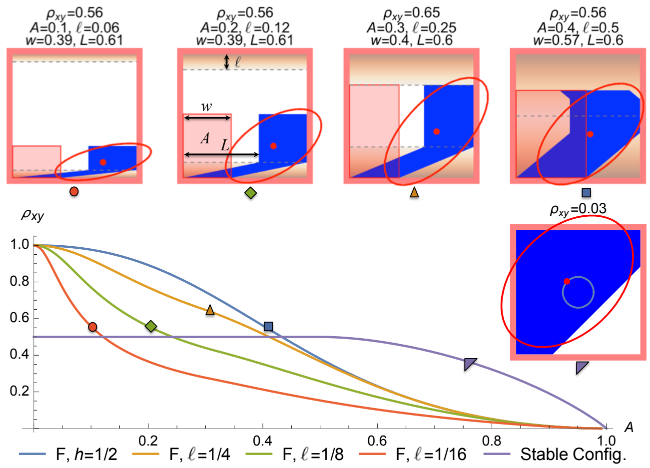

Fig. 8. Analytical results comparing maximum correlation ρ_{xy}. Lines labeled F use the boundary layer friction model of (16) with four boundary layer thicknesses h and the stable triangular configuration (14). ??label rbottom, tleft, rtop

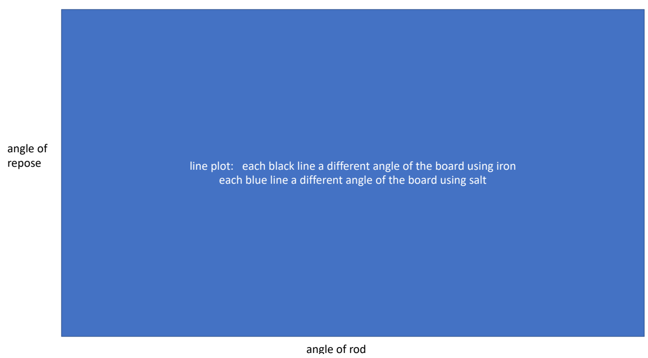

Fig. 9. Experimental data

D. Efficient control of correlation

This section examines maximum correlation values as a function of w, L using (16) from Section IV-C. The maximum correlation using boundary layer friction $\max_{w,L}(\rho(A, h, w, L))$ can be found by gradient descent, as shown in Fig. 8. For swarms with small area, this method enables generating the full range of correlations ± 1. As the swarm area A increases above ≈ 0.43, the stable configuration method is more effective. Larger boundary layers h enable more control of correlation.

V. Experiments

A. Hardware experiment: particle angle of repose

In this section we vary the force and approach angle to shape a swarm with a characteristic angle of repose.

TODO: Haoran will Explain hardware experiment These experiements show how the pile of particles can be used to convey two scalar values: the force applied and the attack angle. We can also apply varying levels of force and torque, as shown in (**??**).

Fig. 10. Magnified image of salt and iron at angle of repose.

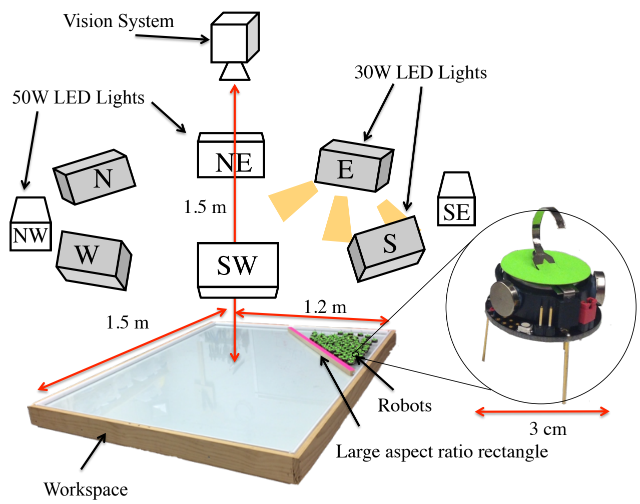

Fig. 11. Hardware platform for steering Kilobots with lights.

B. Hardware experiment: kilobot angle of repose

In this section we vary the force and approach angle to shape a swarm of Kilobots [16] with a characteristic angle of repose. A Kilobot is a three-centimeter diameter, low-cost robot with a light sensor. In our experiments, these robots were programmed to go toward the brightest light in the room. The experimental setup is shown in Fig. 11. Figure 12 shows angle of repose of the Kilobots with three different angles of the pink rod when the rod has 0°, 22.5° and 45°. The green lines show the triangle that the robots pile up. The cyan star is the center of mass of the rod, and mean position and variance of the robots are shown with a red star and red ellipse.

C. Hardware experiment: control of covariance

To demonstrate covariance control, up to 100 kilobots were placed on the workspace and manually steered with lights, using friction with the boundary walls to vary the covariance from -4000 to 3000 cm^2. The resulting covariance is plotted in Fig. 13, along with snapshots of the swarm.

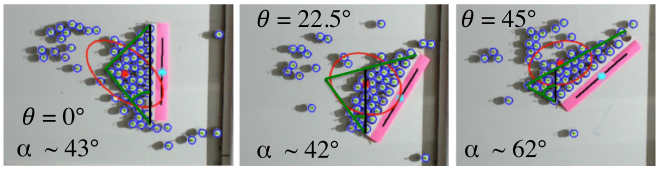

Fig. 12. Angle of repose of Kilobots controlled by light.

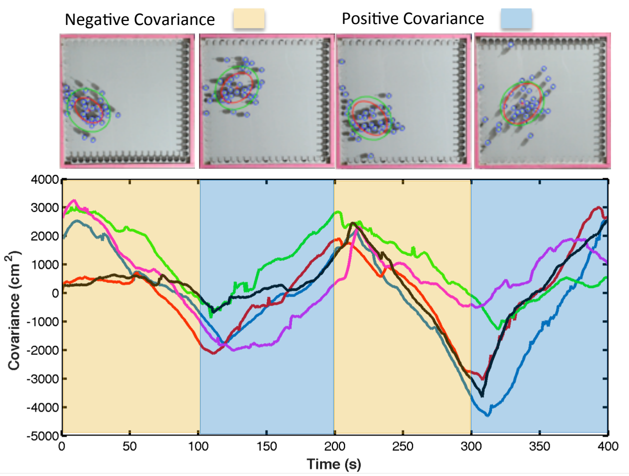

Fig. 13. Hardware demonstration steering ≈ 50 kilobot robots to desired covariance. The goal covariance is negative in first 100 seconds and is positive in the next 100 seconds. The actual covariance is shown in different trials. Frames above the plot show output from machine vision system and an overlaid covariance ellipse.

VI. Conclusion and Future Work

This paper presented techniques for reshaping particles using uniform inputs and non-slip boundary contacts. Hardware experiments illustrated the algorithms in ex vivo and in artificial workspaces.

References

[1] S. Shahrokhi, A. Mahadev, and A. T. Becker, "Algorithms for shaping a particle swarm with a shared input by exploiting non-slip wall contacts," in *Intelligent Robots and Systems (IROS), 2017 IEEE/RSJ International Conference on*, 2017.

[2] S. Shahrokhi, L. Lin, C. Ertel, M. Wan, and A. T. Becker, "Steering a swarm of particles using global inputs and swarm statistics," *IEEE Transactions on Robotics*, vol. 34, no. 1, pp. 207–219, 2018.

[3] A. L. Bertozzi, T. Kolokolnikov, H. Sun, D. Uminsky, and J. Von Brecht, "Ring patterns and their bifurcations in a nonlocal model of biological swarms," *Communications in Mathematical Sciences*, vol. 13, no. 4, pp. 955–985, 2015.

[4] B. R. Donald, C. G. Levey, I. Paprotny, and D. Rus, "Planning and control for microassembly of structures composed of stress-engineered mems microrobots," *The International Journal of Robotics Research*, vol. 32, no. 2, pp. 218–246, 2013. [Online]. Available: http://ijr.sagepub.com/content/32/2/218.abstract

[5] T. Bretl, "Control of many agents using few instructions," in *Proceedings of Robotics: Science and Systems*, Atlanta, GA, USA, June 2007.

[6] A. Becker, C. Onyuksel, T. Bretl, and J. McLurkin, "Controlling many differential-drive robots with uniform control inputs," *The international journal of Robotics Research*, vol. 33, no. 13, pp. 1626–1644, 2014.

[7] Z. Nosrati, N. Li, F. Michaud, S. Ranamukhaarachchi, S. Karagiozov, G. Soulez, S. Martel, K. Saatchi, and U. O. Hfeli, "Development of a coflowing device for the size-controlled preparation of magnetic-polymeric microspheres as embolization agents in magnetic resonance navigation technology," *ACS Biomaterials Science & Engineering*, vol. 4, no. 3, pp. 1092–1102, 2018.

[8] A. Becker, G. Habibi, J. Werfel, M. Rubenstein, and J. McLurkin, "Massive uniform manipulation," in *IEEE International Conference on Intelligent Robots and Systems*, Nov. 2013.

[9] S. Salmanipour and E. Diller, "Eight-degrees-of-freedom remote actuation of small magnetic mechanisms," in *IEEE International Conference on Robotics and Automation*, 2018.

[10] A. Denasi and S. Misra, "Independent and leader follower control for two magnetic micro-agents," *IEEE Robotics and Automation Letters*, vol. 3, no. 1, pp. 218–225, Jan 2018.

[11] E. Diller, J. Giltinan, G. Z. Lum, Z. Ye, and M. Sitti, "Six-degree-of-freedom magnetic actuation for wireless microrobotics," *The International Journal of Robotics Research*, vol. 35, no. 1-3, pp. 114–128, 2016.

[12] H. Zhao and A. T. Becker, "Wolfram demonstrations project: Distribution of a robot swarm in a square under gravity," 2016. [Online]. Available: http://demonstrations.wolfram.com/DistributionOfARobotSwarmInASquareUnderGravity/

[13] ——, "Wolfram demonstrations project: Distribution of a swarm of robots in a circular workplace under gravity," 2016. [Online]. Available: http://demonstrations.wolfram.com/DistributionOfASwarmOfRobotsInACircularWorkplaceUnderGravity/

[14] P. J. Pritchard, *Fox and McDonald's Introduction to Fluid Mechanics, 8th Edition*. John Wiley and sons inc., 2011.

[15] S. Shahrokhi and A. T. Becker, "Stochastic swarm control with global inputs," in *IEEE/RSJ International Conference on Intelligent Robots and Systems (IROS)*. IEEE, 2015, pp. 421–427.

[16] M. Rubenstein, A. Cornejo, and R. Nagpal, "Programmable self-assembly in a thousand-robot swarm," *Science*, vol. 345, no. 6198, pp. 795–799, 2014.